Electron energy levels in $Nd_{2-x}Ce_xCuO_4$: A study by valence- and core-level photoemission spectroscopy

T. R. Cummins
Centre for High Temperature Superconductivity, Department of Chemistry, Imperial College of Science, Technology and Medicine, South Kensington, London SW7 2AY, United Kingdom

R. G. Egdell
Inorganic Chemistry Laboratory, South Parks Road, Oxford OX1 3QR, United Kingdom
(Received 11 January 1993; revised manuscript received 7 April 1993)

Valence- and core-level photoemission spectra of vacuum-annealed polycrystalline $Nd_{2-x}Ce_xCuO_4$ ceramics have been studied over the composition range $0<x<0.20$. The cleaned surfaces give simple O1*s* core line shapes in x-ray photoemission spectroscopy (XPS) and metallic samples with x values in excess of 0.1 display x-ray and Ne(I) excited valence-region spectra showing a distinct Fermi-edge cutoff. Valence-band and core-level binding energies are inconsistent with filling of a rigid conduction band. Moreover, there is little change in the Cu 2*p* XPS line shape across the series. This observation is discussed in relation to the Larsson-Sawatzky model. The Cu 2*p* core-level data for $Nd_{2-x}Ce_xCuO_4$ are compared with those for $La_{2-x}Sr_xCuO_4$. The experimental work reveals a stabilization of Cu 3*d* levels in Nd_2CuO_4 as compared with La_2CuO_4 and suggests a negative charge-transfer parameter Δ in the former compound.

I. INTRODUCTION

The discovery in 1989[1,2] of superconductivity in the phase $Nd_{2-x}Ce_xCuO_4$ aroused widespread interest because simple electron-counting considerations suggest that replacement of trivalent Nd^{III} by formally tetravalent Ce^{IV} should lead to *n*-type doping of the insulating parent compound. In contrast to the *p*-type superconductors, which in general achieve optimal superconducting properties by annealing under oxidizing conditions, $Nd_{2-x}Ce_xCuO_4$ must be postannealed under conditions where oxygen loss from air-sintered samples is possible (e.g., in an Ar or N_2 atmosphere or in vacuum) in order to produce a superconducting material. In addition, Hall effect and Seebeck coefficients are both observed to have signs opposite to those for the more conventional *p*-type oxide superconductors, in agreement with the idea that there are *n*-type carriers.[1-3] Interest therefore focuses on the nature of the charge carriers. In the simplest picture, the parent compound Nd_2CuO_4 is a charge-transfer insulator[4] with any empty upper Hubbard band of dominant Cu 3*d* atomic character lying above a broad O 2*p* band; the lower Cu 3*d* Hubbard band sits in the middle of the O 2*p* band. The added electrons thus occupy the initially empty upper Hubbard band. In a formal bookkeeping sense some of the Cu^{II} has been reduced to the Cu^{I} state. In chemical terms it is, however, difficult to understand the coexistence of Ce^{IV} and Cu^{I}: the redox potentials in aqueous solution[5] ($Ce^{IV}/Ce^{III}=1.70$ V; $Cu^{II}/Cu^{I}=0.159$ V) suggest that Ce^{IV} should oxidize Cu^{I} to Cu^{II}.

Early studies by O*K* edge energy-loss spectroscopy called into question the notion of *n*-type doping and suggested that O 2*p* holes were present even for undoped samples.[6] It was later shown that the pre-edge structure was in fact due to excitation of O 1*s* electrons into a Hubbard band of the dominant Cu 3*d* character strongly admixed with O 2*p* states.[7] The O*K* edge spectra show little change with electron doping. By contrast, pronounced changes in Cu*K* edge x-ray absorption spectra suggest reduction from Cu^{II} to Cu^{I} with Ce doping, although it is controversial as to whether the added electrons should be regarded as localized or itinerant.[8-10] In an elegant and careful experiment, Alexander *et al.*[7] observed that Th^{IV} doping in $Nd_{1.85}Th_{0.15}CuO_4$ causes a 14% reduction in the relative intensity of the excitonic feature in the Cu $2p_{3/2}$ energy-loss spectrum of Nd_2CuO_4. This appears to provide definitive support for the expected increase in the mean 3*d* electron count on copper in this system.

A detailed study of core-level structure in x-ray photoemission provides an alternative and complementary approach to the investigation of the valence states of the various ions in $Nd_{2-x}Ce_xCuO_4$. In particular, for Cu^{II} compounds, the Cu 2*p* core peak contains a "main peak" associated with a well-screened Cu $2p^5 3d^{10}\underline{L}^1$ final state (where $\underline{L}^1$ designates a single hole on the ligand oxygen atom) and a satellite associated with the poorly screened configuration Cu $2p^5 3d^9 \underline{L}^0$. By contrast Cu^{I} gives a single final-state configuration Cu $2p^5 3d^{10}\underline{L}^0$ at an energy close to that of the Cu $2p^5 3d^9\underline{L}^1$ peak for Cu^{II}. Thus the ratio between satellite and main peak intensities should be diagnostic of the Cu oxidation state, reduction from Cu^{II} to Cu^{I} being accompanied by a corresponding reduction in satellite intensity. The first comprehensive study of $Nd_{2-x}Ce_xCuO_4$ core levels was carried out by Ishii *et al.*[11] These workers found that the satellite to main peak intensity ratio in Cu 2*p* x-ray photoemission spectroscopy (XPS) decreased with Ce doping for samples

that had been annealed only in air. However, for "reduced" samples subject to subsequent *ex situ* annealing in Ar, the satellite intensity was constant over the composition range $0.1 < x < 0.2$. Suzuki *et al.*[12] found a similar decrease in satellite intensity for air-annealed samples but studied only a single "reduced" sample with $x = 0.15$. This study was noteworthy for the observation of a nicely defined Fermi-edge structure in x-ray excited valence-region photoemission spectra of samples with $x = 0.15$. Fujimori *et al.*[13] also concentrated on unreduced, air-annealed samples. They found a roughly constant satellite intensity up to $x = 0.15$, with a sudden drop at $x = 0.20$. Their He(II) photoemission spectra showed no indication of a Fermi-edge structure. Finally, Klauda and co-workers[14,15] studied core levels in both unreduced and reduced samples for x values in the range $0 < x < 0.15$. Here the relative satellite intensity decreases with Ce doping for both reduced and unreduced samples. The situation with respect to core-level spectra is thus extremely confusing with no clear consensus in the literature.

The quality of the sample surface is clearly a matter of crucial importance in any photoemission work. In most of the core-level studies alluded to above and in other papers not discussed in detail[16–18] surfaces were prepared by scraping ceramic samples. In all these cases the surfaces have a significant level of residual contamination, as gauged by the appearance of a shoulder on the high binding energy side of the main O 1*s* peak. Suzuki *et al.*[12] argued that low-temperature fracture (the fracture is predominantly intragranular) of ceramic samples provides a route to better quality surfaces, but even these surfaces showed a high binding energy O 1*s* component. Only one paper deals with cleaved single-crystal surfaces but, unfortunately, this is concerned only with valence-band spectra and it is not possible to make contact with the core-level work.[19]

In the present communication we employ an alternative method of surface preparation: high-temperature annealing of ceramic samples under carefully controlled UHV conditions. This method of sample cleaning obviously mimics the reduction step involved in the preparation of superconducting materials within the $Nd_{2-x}Ce_xCuO_4$ phase and is appropriate only for the study of reduced samples. The annealed surfaces differ in principle from cleavage surfaces in that they present atomic distributions which may be brought into thermodynamic equilibrium with the bulk and high-energy steps and defects that may be present on cleavage surfaces are healed during the annealing process. Sakisaka *et al.*[20] have used a closely related procedure to prepare clean, ordered, thin-film (001) single-crystal surfaces for ultraviolet valence-region photoemission studies. Confidence in the approach can be drawn from the very high quality of the photoemission spectra obtained by them and their observation of sharp (1×1) low-energy electron diffraction (LEED) patterns. In fact, the definition of structure close to the Fermi energy is much better in their work than for surfaces prepared by any other means, including cleavage of single crystals.[19] In our own hands, UHV annealing leads to atomically clean surfaces with O 1*s* XPS line shapes free of high binding energy shoulders. As noted by Fowler *et al.*, appraisal of the photoemission studies is often hampered by "selective" reporting of the available data and a failure to quantify the level of C surface contamination.[21] In the present paper we make a full presentation of core-level spectra. By working on well-defined surfaces of this sort we are able to explore the new physics to emerge from our data with some confidence.

The work on Nd_2CuO_4 is extended to include comparison with La_2CuO_4 and $La_{1.85}Sr_{0.15}CuO_4$. There has been little photoemission work on this system in the past two years but there is no obvious consensus in the literature about the effects of Sr doping on Cu core-level spectra.

II. EXPERIMENTAL

Samples within the series $Nd_{2-x}Ce_xCuO_4$ ($x = 0.00$, 0.05, 0.10, 0.15, and 0.20) were prepared by firing finely ground mixtures of Nd_2O_3 (Aldrich 99.99%), CuO (Aldridge 99.999%), and CeO_2 together at 1050 °C in air for 5 days with intermediate regrindings.[1,2] The CeO_2 was itself freshly prepared by thermal decomposition of $Ce(CO_3)_2$ (Aldridge 99.99%) at 900 °C.[22] Samples were then pelletized and refired in flowing He (BOC Secial Gases Zero Grade) at 910 °C for 16 h and quenched to room temperature under a sustained He flow. Samples were subject to a final anneal in flowing He at 550 °C, as recommended by Takagi, Uchida, and Tokura.[2]

X-ray powder diffraction patterns of samples prepared in this way contained only reflections characteristic of the tetragonal T' phase. The c-axis lattice parameter decreased smoothly from 12.18 to 12.06 Å as x varied from 0.00 to 0.20, while the basal plane parameter a showed a small but progressive increase from 3.943 to 3.945 Å.

Samples with $x = 0$, 0.05, and 0.10 showed activated conduction with no transition to a superconducting state. $Nd_{1.85}Ce_{0.15}CuO_4$ showed an almost temperature-independent normal state conductivity, with a superconducting onset at 23 K and zero resistance at 20 K. $Nd_{1.8}Ce_{0.2}CuO_4$ showed nonactivated conduction but did not undergo a superconducting transition at temperatures above 13 K.

Photoemission spectra were measured in a two-chamber VG ESCALAB 5 Mark II spectrometer. The main chamber (base pressure 8×10^{-11} mbar) was equipped with a 150 mm mean radius spherical sector electron energy analyzer, twin anode (Mg, Al) x-ray source and high-intensity noble gas discharge lamp. The analyzer resolution was set at 0.4 eV for x-ray and He(II) excited spectra and at 0.1 eV for spectra excited with He(I) and Ne(I) radiation. Samples were mounted on stainless-steel stubs and held in place by stainless-steel clips.

As-prepared samples showed prounced C 1*s* intensity in XPS (Fig. 1) and gave an O 1*s* signal with a strong high binding energy shoulder (Fig. 2). *In situ* cleaning of the $Nd_{2-x}Ce_xCuO_4$ ceramics was effected by annealing in UHV (base pressure 5×10^{-10} mbar) at 550 °C with the

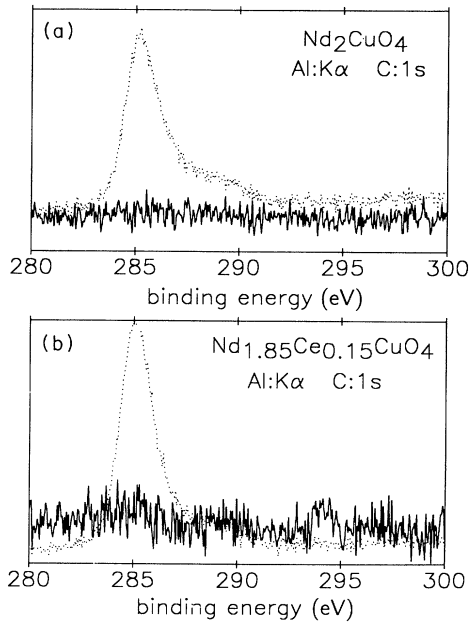

FIG. 1. Al $K\alpha$ core-level XPS in C 1s region for (a) Nd_2CuO_4 and (b) $Nd_{1.85}Ce_{0.15}CuO_4$ for as-prepared samples (dots) and after *in situ* cleaning (solid lines).

aid of a 1.5 kW rf generator coupled to the sample and its stub by a water-cooled copper workcoil.[23] The surface temperature during the annealing treatment was measured by an emissivity calibrated infrared pyrometer. After a pressure rise to about 10^{-7} mbar, associated with desorption of contaminants, the base pressure was recovered after around 2–3 h sustained annealing. After this *in situ* treatment, the C 1s level was reduced below the limit of detectability in XPS (Fig. 1) and the high binding energy shoulder on the O 1s core line was essentially eliminated (Fig. 2). As emphasized in Figs. 1 and 2, this pretreatment is effective at removing surface contaminants for both doped and undoped samples.

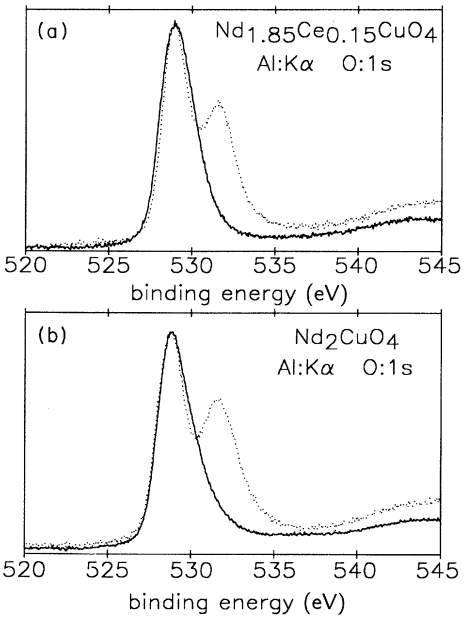

FIG. 2. Al $K\alpha$ core-level XPS in O 1s region for (a) $Nd_{1.85}Ce_{0.15}CuO_4$ and (b) Nd_2CuO_4 for as-prepared samples (dots) and after *in situ* cleaning (solid lines).

La_2CuO_4 and $La_{1.85}Sr_{0.15}CuO_4$were prepared by standard techniques.[24] *In situ* cleaning for these samples involved annealing in the ESCALAB preparation chamber under 1 atm of pure oxygen (BOC zero grade) at 600 °C. This cleaning procedure yielded single-peak O 1s core-level spectra,[23] vanishingly low levels of C contamination of He(III) spectra free of adsorbate peaks around 9.5 eV: the data were comparable in these respects to that for Nd_2CuO_4.

III. RESULTS AND DISCUSSION

A. Valence-level spectra of $Nd_{2-x}Ce_xCuO_4$

Consideration of experimental data begins with discussion of valence-level spectra, because these provide a critical benchmark as to the quality of the sample surface. In particular, we regarded the presence of the expected Fermi-edge cutoff in x-ray excited valence-band spectra of metallic samples and the absence of peaks due to adsorbates at 9–10 eV binding energy in He(II) spectra as prerequisite indicators of a successful cleaning cycle. Figures 3–6 show valence-region spectra excited with Ne(I) (Fig. 3, $h\nu=16.8$ eV), He(I) (Fig. 4, $h\nu=21.2$ eV), He(II) (Fig. 5, $h\nu=40.8$ eV), and Al$K\alpha$ (Fig. 6, $h\nu=1486.6$ eV) radiation.

Optimal surface sensitivity and separation between valence-band structure itself and secondary electron structure is achieved in He(II) spectra (Fig. 5). There is no indication in these data of structure to the high binding energy side of the main valence band associated with unwanted adsorbates. For $YBa_2Cu_3O_7$ (Ref. 25) and La_2CuO_4 (Ref. 26) it is now generally accepted that structure below the main valence band [other than that due to Cu $3d^8$ valence-band satellites] is associated with poor surface quality or surface adsorbates and similar consideration must apply to $Nd_{2-x}Ce_xCuO_4$. It is surprising then that most published photoemission spectra, including those of Grassman *et al.*,[14] Hwu *et al.*,[27] Reihl *et al.*,[28] and Sakisaka *et al.*[20] show a strong adsorbate-related structure at around 9–10 eV.

The main valence-band onset in He(II) photoemission spectra is about 0.75 eV below the Fermi level for the parent Nd_2CuO_4. This compares with the bulk charge-transfer gap of about 1.5 eV.[29] The overall valence bandwidth in He(II) spectra is of the order of 8 eV. The bandwidth is similar in Al $K\alpha$ spectra (Fig. 6). Moreover, there is no major change in spectral profiles on changing from excitation at 40.8 to 1486.6 eV. Across this photon energy range there are very pronounced changes in the ionization cross sections[30] for the atomic states contributing to the valence-band intensity (Table I). At the lower photon energy, the spectra should be dominated by the O 2p partial density of states, but at the higher x-ray energy

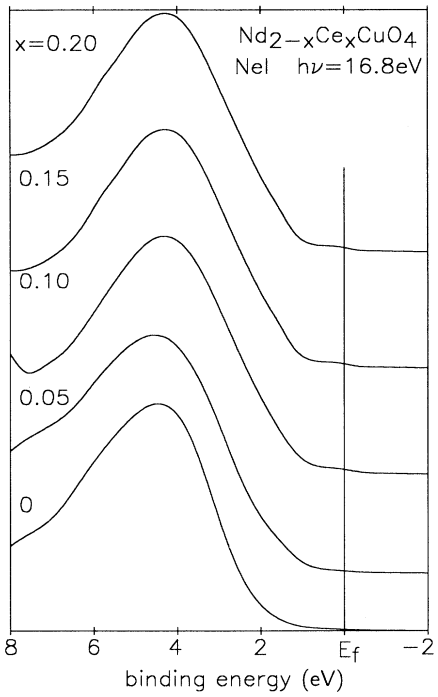

FIG. 3. Valence-region photoelectron spectra of $Nd_{2-x}Ce_xCuO_4$ excited with Ne(I) radiation: $h\nu=16.8$ eV. Binding energies are given relative to the Fermi energy of the metallic sample stub. Binding energy scales in the other valence-band spectra are also defined in this way.

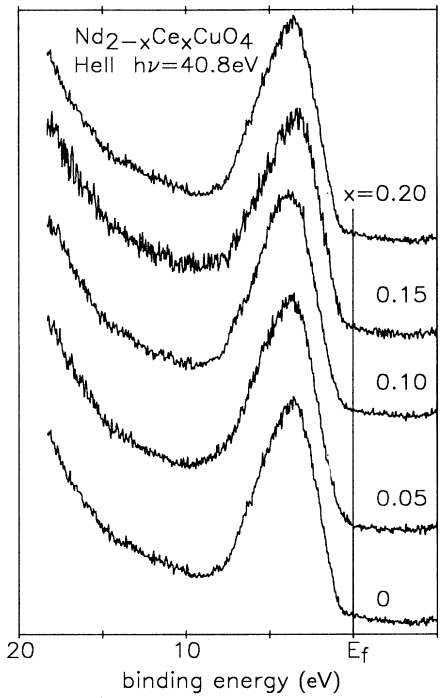

FIG. 5. Valence-region photoelectron spectra of $Nd_{2-x}Ce_xCuO_4$ excited with He(II) radiation: $h\nu=40.8$ eV. Structure due to He(II)β and He(II)γ radiation has been subtracted.

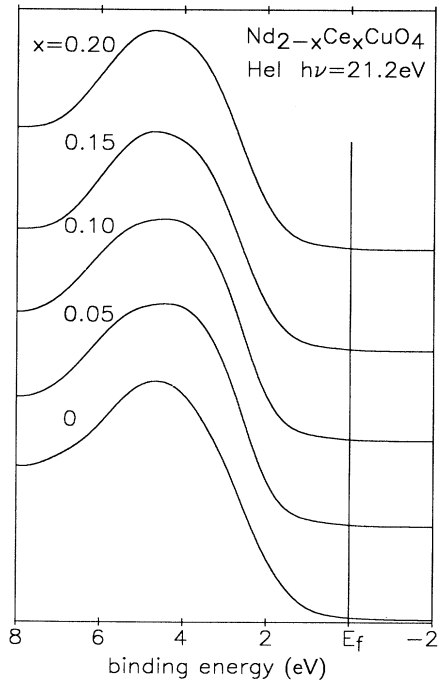

FIG. 4. Valence-region photoelectron spectra of $Nd_{2-x}Cu_xCuO_4$ excited with He(I) radiation: $h\nu=21.2$ eV. Structure due to He(I)β and He(I)γ satellite radiation has been subtracted from the spectra.

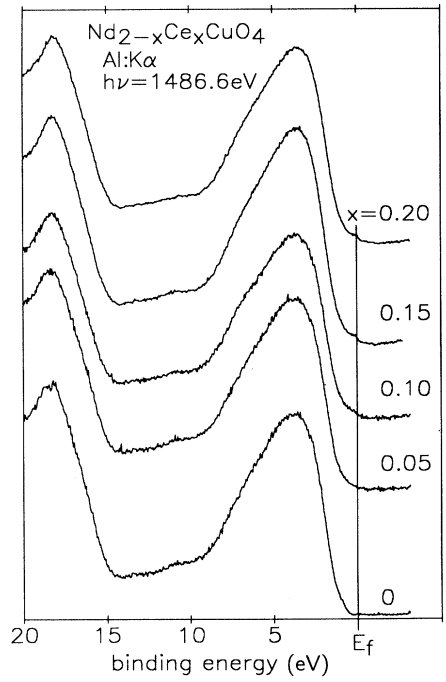

FIG. 6. Valence-region photoelectron spectra of $Nd_{2-x}Ce_xCuO_4$ excited with Al$K\alpha$ radiation: $h\nu=1486.6$ eV. Structure due to satellite radiation has been subtracted from the spectra.

TABLE I. One-electron ionization cross sections (σ) and fractional contributions (I) to total valence-band intensity for occupied valence levels of La_2CuO_4 and Nd_2CuO_4 at differing photon energies.

$h\nu$ (eV)	16.8	21.2	40.8	1486.6
σ(Nd 4f)/Mb	1.04×10^{-1}	1.74×10^{-1}	7.08×10^{-1}	1.58×10^{-3}
σ(Cu 3d)/Mb	6.45×10^{-1}	7.55×10^{-1}	9.93×10^{-1}	1.20×10^{-3}
σ(O 2p)/Mb	2.61	2.67	1.70	6.0×10^{-5}
La_2CuO_4				
I(Cu 3d)	0.085	0.096	0.180	0.882
I(O 2p)	0.915	0.904	0.820	0.118
Nd_2CuO_4				
I(Nd 4f)	0.005	0.007	0.041	0.187
I(Cu 3d)	0.084	0.095	0.172	0.738
I(O 2p)	0.911	0.898	0.787	0.075

the major contribution to the spectral intensity comes from the Cu 3d partial density of states (with a small but significant contribution from Nd 4f states). The lack of major changes in the spectral profiles therefore indicates that there is very substantial mixing between Cu 3d and O 2p states, with relatively little change in atomic composition across the band.

Next we consider changes in spectra with doping. In a rigid band model, n-type doping into the upper Cu 3d Hubbard band should lead to a shift of valence-band features to *higher* binding energy and to the appearance of a conduction-band peak separated from the main valence band. There is no indication of such a shift. Instead, at the lowest photon energy ($h\nu=16.8$ eV, Fig. 3), there is some indication of broadening of the valence-band edge toward the Fermi level with Ce doping, and a very small (0.2 eV) shift to *lower* binding energy for the valence-band maximum as x in $Nd_{2-x}Ce_xCuO_4$ varies from $x=0.0$ to 0.2. This is in contrast to the downward band shift observed by Reihl *et al.*,[28] although we draw attention to the very high intensity of the contaminant structure in the He(II) spectra of this earlier work. The lack of shift is in fact more in keeping with the data of Allen *et al.*,[19] who overlaid valence-band spectra of Nd_2CuO_4 and $Nd_{1.85}Ce_{0.15}CuO_4$ excited with synchrotron radiation at $h\nu=72$ eV. There was no discernible shift in the valence-band maximum, but a small broadening of the valence-band edge. We return to discussion of the rigid band model in the context of comparison of data for $Nd_{1.85}Ce_{0.15}CuO_4$ and $La_{1.85}Sr_{0.15}CuO_4$.

Turning next to the states at the Fermi energy itself, a weak but well-defined Fermi-edge cutoff structure is found in Ne(I) and Al$K\alpha$ excited spectra. Note, however, that the photoemission intensity at E_f in Ne(I) spectra continues down to the main valence-band onset and there is no well-defined gap between "valence" and "conduction" bands (Fig. 7). The intensity close to E_f is very low at $h\nu=21.2$ and 40.8 eV. The 21.2 eV data are in agreement with the experiments of Sakisaka *et al.*,[20] who found vanishing Fermi energy intensity below $h\nu=30$ eV, with a very strong maximum in the Fermi energy intensity at $h\nu=50$ eV. These variations were interpreted in terms of the one-electron cross-section profile for Cu 3d states, although the experimental intensity peaked much more strongly than the atomic cross-section profile. Allen *et al.*[19] studied the Fermi-level intensity in the energy range 40 eV $< h\nu <$ 140 eV and found a less sharp maximum at $h\nu=50$ eV and antiresonance behavior around the Cu 3p core threshold at $h\nu=74$ eV. This again conforms to the pattern expected for states of dominant Cu 3d atomic character. The high Fermi energy intensity of $h\nu=16.8$ eV is thus somewhat puzzling when viewed in the context of previous photoemission experi-

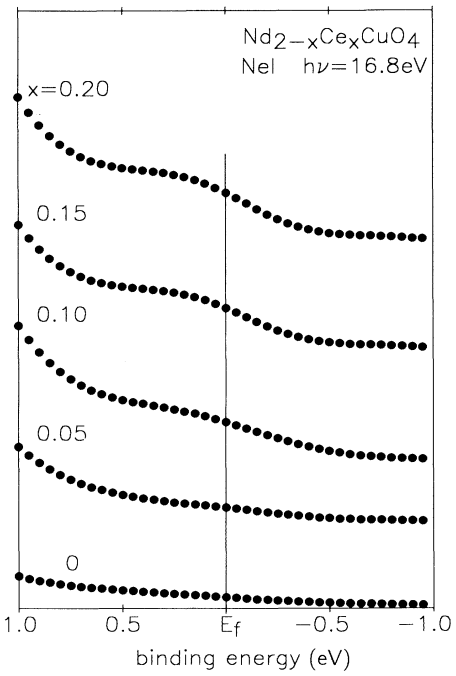

FIG. 7. Ne(I) photoemission spectra ($h\nu=16.8$ eV) of $Nd_{2-x}Ce_xCuO_4$ in the region close to the Fermi energy. The intensity has been normalized relative to the valence-band maximum.

ments. However, it is important to recognize that due to covalency the states at E_f must have very substantial O $2p$ as well as Cu $3d$ atomic character. In addition, it is well known that the inelastic mean-free-path length for electrons in solids increases strongly at low photon energies,[31] so that photoemission measurements at $h\nu=16.8$ eV are intrinsically less surface sensitive than at the higher energies. Thus if the density of states at E_f, $N(E_f)$, is depressed in the near surface region over distances of the order of electron pathlengths, enhanced Fermi energy intensity will be found on increasing the path length.

There are, in turn, at least three potential mechanisms for suppression in $N(E_f)$ at the surface. First, there is the possibility of poor surface quality. It would be dangerous to discount this consideration although the clean O $1s$ line shape argues against it. Second, there may be "desegregation" of Ce with a reduced Ce/Nd ratio and correspondingly lower n-type carrier concentration near the surface. However, we can discount this possibility because the Ce/Nd core-level intensity ratio shows no obvious change with the change in angle of the off take of photoelectrons (Sec. III C). Finally, there is the possibility of an "intrinsic" suppression in the density of states close to the surface due to band narrowing and enhanced tendency toward localization of the n-type carriers into states falling below the bulk conduction band, due, for example, to trapping as small polarons.[32]

B. Comparison of valence-level spectra of $La_{2-x}Sr_xCuO_4$ and $Nd_{2-x}Ce_xCuO_4$

Ne(I) photoemission spectra of oxygen-annealed La_2CuO_4 and $La_{1.85}Sr_{0.15}CuO_4$ are shown in Fig. 8. The p-type doping leads in this system to the appearance of a well-defined Fermi-edge structure, as emphasized in Fig. 9, which shows expanded scans close to the Fermi energy. As with the Nd_2CuO_4 system, we fail to observe the shift in the position of the valence-band maximum which would be expected on the basis of a rigid band model. This is at variance with the shift of the valence-band

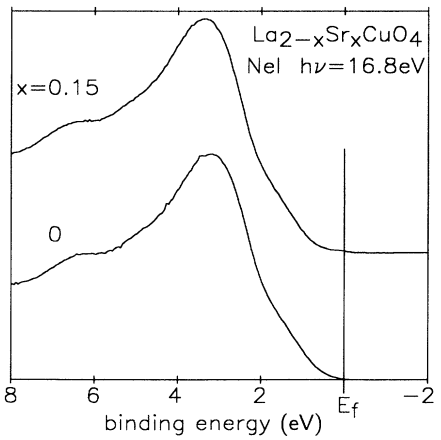

FIG. 8. Ne(I) photoemission spectra ($h\nu=16.8$ eV) of La_2CuO_4 and $La_{1.85}Sr_{0.15}CuO_4$.

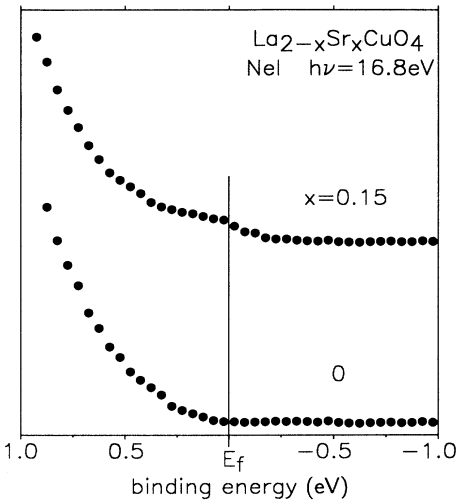

FIG. 9. Ne(I) photoemission spectra ($h\nu=16.8$ eV) of La_2CuO_4 and $La_{1.85}Sr_{0.15}CuO_4$ in the region close to the Fermi energy. The intensity has been normalized relative to the valence-band maximum.

structure toward the Fermi level with hole doping observed by Shen *et al.*[33] in $Bi_2Sr_2CaCu_2O_8$. However, the lack of rigid band shifts is in accord with previous photoemission work on the closely related perovskite material $La_{1-x}Sr_xVO_3$ (Ref. 34) that undergoes a metal to nonmetal transition with increasing hole doping. There is also no indication of a rigid band shift in inverse photoemission spectra $La_{2-x}Sr_xNiO_4$.[35]

Although within the two series $La_{2-x}Sr_xCuO_4$ and $Nd_{2-x}Ce_xCuO_4$ the separation between valence-band structure and the Fermi energy remains fixed, the valence-band structures for the two series do not coincide. This is illustrated in Fig. 10 which shows superim-

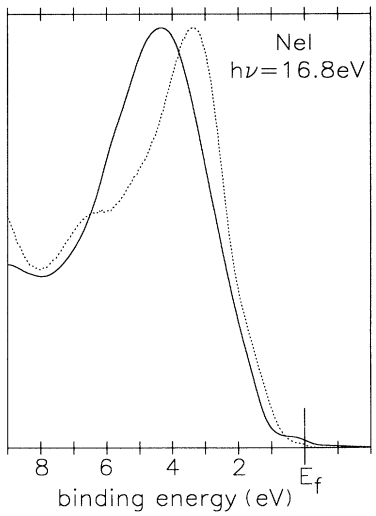

FIG. 10. Comparison between Ne(I) excited photoemission spectra of $La_{1.85}Sr_{0.15}CuO_4$ (dashed line) and $Nd_{1.85}Ce_{0.15}CuO_4$ (solid line).

posed Ne(I) excited spectra of $La_{1.85}Sr_{0.15}CuO_4$ and $Nd_{1.85}Ce_{0.15}CuO_4$: these are chosen rather than the parent undoped species because the position of the Fermi energy is unambiguously defined by the observed Fermi-Dirac cutoff in the photoemission profile. However, a similar picture pertains for the undoped parents. It is clear from Fig. 10 that the valence band is shifted downward in energy relative to the Fermi energy for $Nd_{1.85}Ce_{0.15}CuO_4$ as compared with $La_{1.85}Sr_{0.15}CuO_4$. In contrast to Allen *et al.*[19] we cannot therefore put forward a model where doping is into "midgap" states at the same energy for both La_2CuO_4 and Nd_2CuO_4. Instead, we envisage that in the undoped compounds the Fermi levels are pinned at different positions by impurity states for the parent compounds, i.e., for La_2CuO_4 the Fermi level is pushed into the lower half of the charge-transfer gap due to formation of Zhang-Rice singlet states[36] by low concentrations of *p*-type carriers, while for Nd_2CuO_4 the Fermi level sits just below the bottom of the upper Hubbard band at the top of the charge-transfer gap. In addition, it must be remembered that the charge-transfer gap is smaller for Nd_2CuO_4 than for La_2CuO_4 (Refs. 29, 37, and 38) so that the change in position of the Fermi energy cannot be equated with the charge-transfer gap of either compound taken alone. In agreement with this broad picture, the O 1*s* core level binding energy shows a shift to lower binding energy for the $La_{2-x}Sr_xCuO_4$ series as compared with the $Nd_{2-x}Ce_xCuO_4$ series (see below), although the shift of ~ 0.3 eV is somewhat smaller than expected.

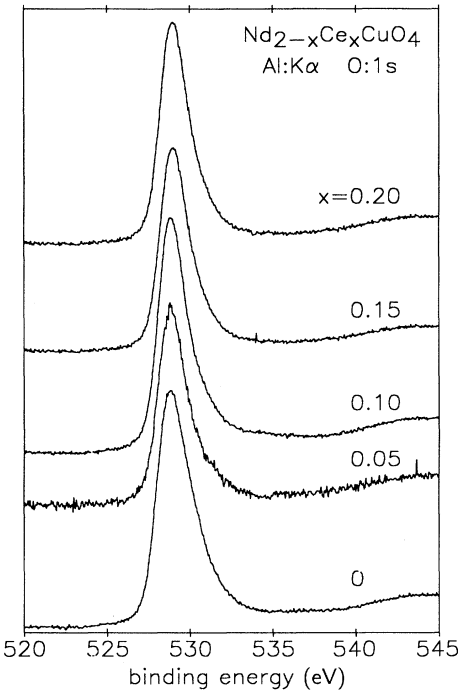

FIG. 11. Al $K\alpha$ excited photoemission spectra of compounds within the series $Nd_{2-x}Ce_xCuO_4$ in the O 1*s* region. Structure due to satellite radiation has been subtracted from the spectra. Note the clean O 1*s* line shape and the lack of shift of peak position with Ce doping.

C. Core-level spectra of $Nd_{2-x}Ce_xCuO_4$: O 1*s*, Nd 3*d*, and Ce 3*d* regions

The O 1*s* spectra for the series $Nd_{2-x}Ce_xCuO_4$ in Fig. 11 demonstrate the efficacy of the sample cleaning procedure across the complete composition range studied. The O 1*s* binding energy is essentially fixed at 528.8 ± 0.1 eV (Table II). The constant binding energy is inconsistent with rigid band filling of an upper Hubbard band and reinforces the conclusion from valence-band studies that this model is inappropriate to describe electron doping in Nd_2CuO_4. The fact that we are able to obtain clean O 1*s* core line shapes is crucial to exploring the applicability of the rigid band model by core-level photoemission spectroscopy because the other core levels display complex line shapes due to a variety of many electron processes, as will emerge below.

Consider next the Nd 3*d* core levels (Fig. 12). Each of the two spin-orbit components of this core level is characterized by a shoulder to the low binding energy side of the main peak. The ground state of Nd^{III} is well described with a relatively pure $4f^3$ valence shell configuration, but due to the strong 3*d* core hole 4*f*

TABLE II. Core electron binding energies for $Nd_{2-x}Ce_xCuO_4$ and $La_{2-x}Sr_xCuO_4$. All values in eV.

x	O 1*s*	Cu $2p_{3/2}$	Nd $3d_{5/2}$	Ce $3d_{5/2}$		
				v	v''	v'''
$Nd_{2-x}Ce_xCuO_4$						
0.00	528.8	932.8	981.7			
0.05	528.8	932.7	981.5			
0.10	528.8	932.8	981.5			
0.15	528.9	932.8	981.3	881.4	887.9	899.6
0.20	528.7	932.8	981.1	881.3	887.8	899.5
$La_{2-x}Sr_xCuO_4$						
0	528.4	932.7				
0.15	528.5	932.7				

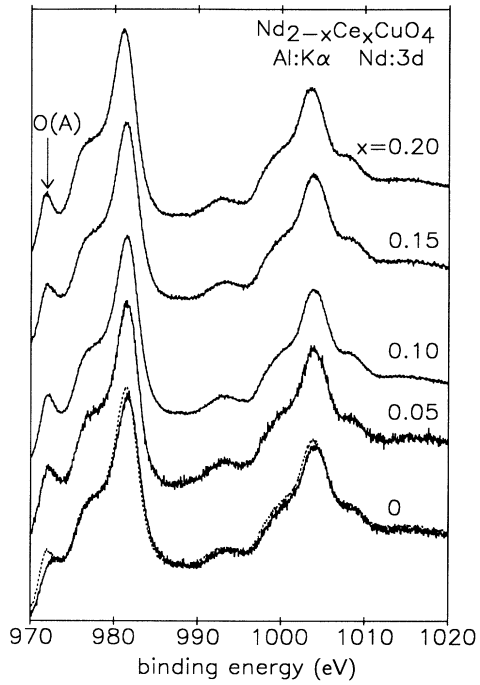

FIG. 12. Al $K\alpha$ excited photoemission spectra of compounds within the series $Nd_{2-x}Ce_xCuO_4$ in the Nd $3d$ region. Structure due to satellite radiation has been subtracted from the spectra. The peak labeled O(A) is due to *OKLL* Auger emission. The spectrum for $x=0.20$ (dashed line) has been overlaid on the spectrum for $x=0.00$ in the bottom panel.

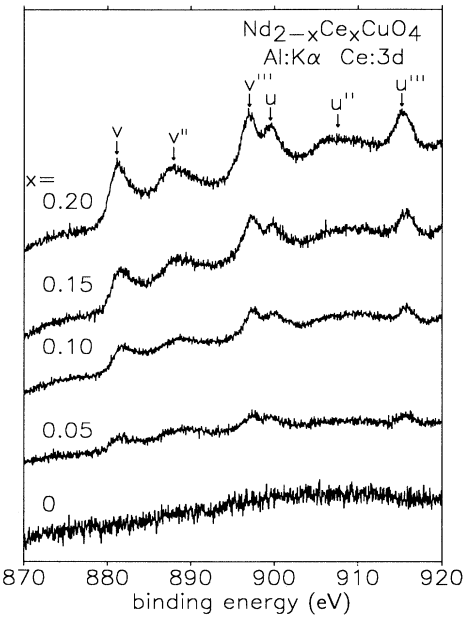

FIG. 13. Al$K\alpha$ excited photoemission spectra of compounds within the series $Nd_{2-x}Ce_xCuO_4$ in the Ce $3d$ region. Structure due to satellite radiation has been subtracted from the spectra. The intensity has been normalized by reference to the Nd $3d$ intensity. The notation v, v'', etc. is discussed in the text.

Coulomb attraction, the $4f$ levels are pulled down in the final state. This allows appearance of a screened final state in which an electron is transferred from the ligand (L=oxygen) level into the $4f$ shell to give a final-state valence shell configuration $4f^4\underline{L}^1$ (where the bar indicates a hole on the ligand).[39] This is responsible for the low binding energy shoulder. In addition, the $3d_{5/2}$ peak has a satellite to higher binding energy close to the foot of the $3d_{3/2}$ peak. This was assigned by Klauda and coworkers[14,15] to a final-state $4f^2$ configuration. A similar structure appears in the $4d$ core-level spectrum of Nd_2O_3 and is apparently associated with electrostatic coupling between the core hole and the outer $4f^3$ electrons, rather than with a descreened $4f^2$ configuration.[40] In agreement with Klauda *et al.*[15] we find that with Ce doping, the intensity ratio $I(4f^3)/I(4f^4\underline{L}^1)$ increases. This suggests decreasing $4f$-O $2p$ covalency due to competition from the more acidic Ce^{IV} ions and less efficient final-state screening by charge transfer from oxygen. In addition, there is a progressive and well-defined downward shift in the binding energy of the main $4f^3$ peak with Ce doping. This is again consistent with a decrease in the transfer integral $\langle 4f^3|H|4f^4\underline{L}^1\rangle$ with increasing Ce doping.

The Ce $3d$ core-level spectrum itself shows a complex six-line pattern (Fig. 13). The spectral intensity increases with Ce doping and the intensity ratio I(Ce $3d$)/I(Nd $3d$) is, after correction for atomic sensitivity factors, close to the value expected from the nominal bulk doping level (Table III). The distinct six-line pattern observed at $x=0.20$ persists down to the lowest doping level and across the complete composition range studied it bears a striking qualitative similarity to the Ce $3d$ spectrum of CeO_2. In discussing this spectrum we label the six peaks v, v'', v''', u, u'', and u''', in accordance with the notation introduced by Burroughs *et al.* in their pioneering XPS study of this compound.[41] Assignment of the spectrum has proved to be controversial,[42] but following Kotani and co-workers[43,44] and Fujimori[45,46] the following interpretation can be given. Due to Ce $4f$-O $2p$ covalency, the ground state in CeO_2 must be regarded as a linear combination of $4f^0$ and $4f^1\underline{L}^1$ configurations. The Coulomb interaction between the $4f$ levels and the $3d$ core hole allows three distinct valence shell final-state configurations to appear in XPS. These are $4f^0$, $4f^1\underline{L}^1$, and $4f^2\underline{L}^2$. The bare $4f^0$ configuration lies at the highest binding energy with $4f^2\underline{L}^2$ below $4f^1\underline{L}^1$. Thus the six lines are assigned as follows:

$$v(\underline{3d}_{5/2}{}^1 4f^1\underline{L}^1),\quad v''(\underline{3d}_{5/2}{}^1 4f^2\underline{L}^2),$$
$$v'''(\underline{3d}_{5/2}{}^1 4f^0),\quad u(\underline{3d}_{3/2}{}^1 4f^1\underline{L}^1),$$
$$u''(\underline{3d}_{3/2}{}^1 4f^2\underline{L}^2),\quad u'''(\underline{3d}_{3/2}{}^1 4f^0).$$

Here the underbar designates a core- or valence-level hole. Ce_2O_3 differs from CeO_2 in that the ground state is a relatively pure $4f^1$ configuration and only two possible final states are possible. These are the unscreened configuration $4f^1$ and the screened configuration $4f^2\underline{L}^1$.

TABLE III. Cu $2p_{3/2}$ satellite intensities and energies and model parameters for La_2CuO_4 and Nd_2CuO_4 in the Larsson-Sawatzky model. The bold values correspond to the same value of Q for both compounds. The effect of reducing Q for Nd_2CuO_4 is also shown. The formally acceptable set of parameters shown in parentheses for Nd_2CuO_4 is not believed to be physically realistic (see text).

	W(eV)	I_s/I_m	Q(eV)	Δ(eV)	T(eV)
La_2CuO_4	8.6	0.41	**7.9**	**0.8**	**2.4**
Nd_2CuO_4	9.1	0.26	**7.9**	**−0.9**	**1.2**
			(7.9	+3.8	2.9)
			7.8	−0.9	1.4
			7.7	−0.9	1.5
			7.6	−0.8	1.8
			7.5	−0.7	2.0
			7.4	−0.2	2.5

The absence of the "bare" $4f^0$ configuration is diagnostic of a Ce^{III} ground state.[39,43] The present data is thus important in establishing for the first time that at all Ce doping levels, the Ce is substituting as Ce^{IV} rather than Ce^{III}, even in reduced samples.

D. Cu 2p core-level spectra of $Nd_{2-x}Ce_xCuO_4$ and comparisons with $La_{2-x}Sr_xCuO_4$

Cu $2p_{3/2}$ core-level spectra for reduced vacuum-annealed samples of $Nd_{2-x}Ce_xCuO_4$ ($x=0$, 0.05, 0.1, 0.15, and 0.2) are shown in Fig. 14. As with other copper oxide superconductors, a two-peak structure is observed. There is, however, little change in the peak profiles with Ce doping, as emphasized in Fig. 15 which shows spectra of Nd_2CuO_4 and $Nd_{1.8}Ce_{0.20}CuO_4$ overlaid. This contrasts with the situation for $La_{2-x}Sr_xCuO_4$, where Sr doping leads to a broadening of the low binding energy peak and a general shift in spectral weight to high binding energy (Fig. 16). It is also striking in comparing data for $Nd_{2-x}Ce_xCuO_4$ and $La_{2-x}Sr_xCuO_4$ that the high binding energy satellite peak is much weaker in the former series and has a greater separation from the main peak.

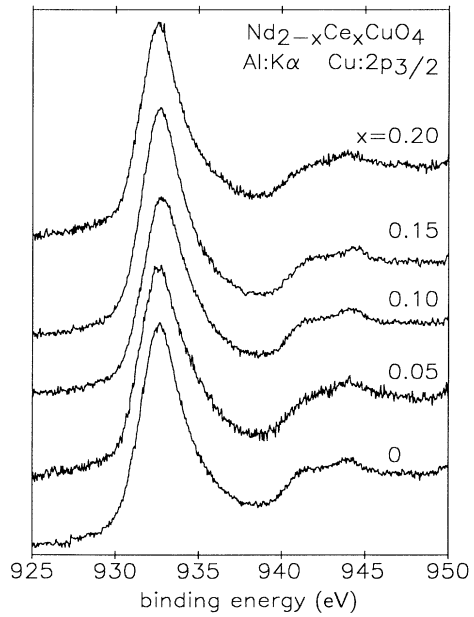

FIG. 14. Al$K\alpha$ excited photoemission spectra of compounds within the series $Nd_{2-x}Ce_xCuO_4$ in the Cu $2p_{3/2}$ region. Structure due to satellite radiation has been subtracted from the spectra.

Consider first the parent undoped compounds. In terms of the Larsson-Sawatzky model,[47–52] the two-peak structure arises as follows. In a purely ionic system, the initial state corresponds to a $3d^9$ valence configuration on copper. To incorporate the effects of covalency a second configuration $3d^{10}\underline{L}^1$ is introduced, where $\underline{L}^1$ corresponds to a hole on the ligand (oxygen) atoms surrounding the Cu. The energy Δ between these configurations is given by

$$\Delta = E(|3d^{10}\underline{L}^1\rangle) - E(|3d^9\rangle) . \quad (1)$$

The two configurations interact through a transfer integral T defined by

$$T = \langle 3d^9|H|3d^{10}\underline{L}^1\rangle \quad (2)$$

to give a ground state whose wave function is

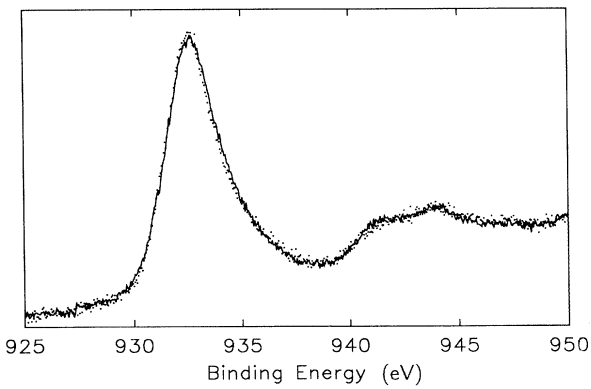

FIG. 15. Overlaid Al$K\alpha$ excited photoemission spectra of Nd_2CuO_4 (solid line) and $Nd_{1.8}Ce_{0.2}CuO_4$ (dots) in the Cu $2p_{3/2}$ region.

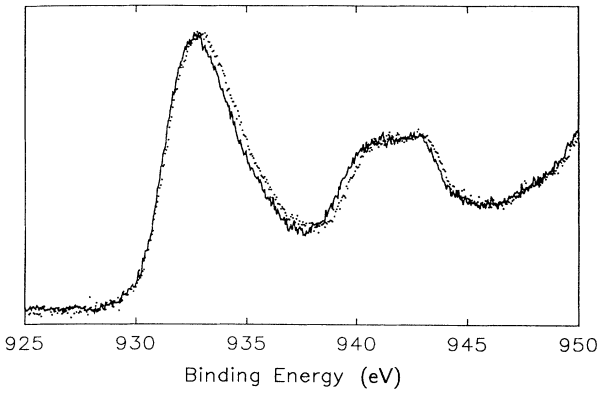

FIG. 16. Overlaid Al $K\alpha$ excited photoemission spectra of La_2CuO_4 (solid line) and $La_{1.85}Sr_{0.15}CuO_4$ (dots) in the Cu $2p_{3/2}$ region.

$$\Psi_G = \cos\theta|3d^9\rangle - \sin\theta|3d^{10}\underline{L}^1\rangle \ , \tag{3}$$

where

$$\tan 2\theta = 2T/\Delta \quad \text{with } 0 < 2\theta < \pi \ . \tag{4}$$

Note that $\Delta > 0$ gives a ground state of a dominant $3d^9$ character, whereas for $\Delta < 0$ the ground state has a dominant $3d^{10}\underline{L}^1$ character. In the final state in XPS, the Cu $2p$ core hole stabilizes the $3d^9$ configuration relative to the $3d^{10}\underline{L}^1$ configuration by an energy Q: for $Q > \Delta$ and $\Delta > 0$ the ordering of configurations in the final state is different to that in the initial state. Due to the change in hybridization between the two configurations, two final states now appear in XPS with an energy separation W:

$$W = [(\Delta - Q)^2 + 4T^2]^{1/2} \tag{5}$$

and an intensity ratio between the low binding energy peak (usually referred to as the main peak m) and the high binding energy peak (usually referred to as the satellite peak s) I_s/I_m, where

$$I_s/I_m = \tan^2(\theta' - \theta) \ , \tag{6}$$

$$\tan 2\theta' = 2T/(\Delta - Q) \quad \text{with } 0 < 2\theta' < \pi \ . \tag{7}$$

We have investigated the variation of W and I_s/I_m with Δ and T for various physically realistic values of the core-valence Coulomb interaction parameter Q in the range between 7 and 9 eV. In general, the satellite intensity decreases with decreasing Δ and is particularly low for $\Delta < 0$, i.e., in situations where $d^{10}\underline{L}^1$ already lies below d^9 in the initial state and the core-hole Coulomb potential does not reverse the order of the configurations. Moreover, negative Δ values lead to large W values.

Since there are three variable parameters and only two observables (the relative satellite intensity and energy), there is no unique way to derive parameters in the model from experimental data. We have explored all possible solutions consistent with the experimental Cu $2p_{3/2}$ core-level data for La_2CuO_4 and Nd_2CuO_4 subject only to the broad constraints that -1 eV $< \Delta < 3$ eV, 0.5 eV $< T < 4$ eV, and 0 eV $< Q < 20$ eV. Solutions for Nd_2CuO_4 exist only for Q values in the range 7.4–7.9 eV and for La_2CuO_4 in the range 7.8–8.3 eV. Of course Q is essentially an atomic parameter and it is T and Δ which are of greater interest in relation to the valence electronic structure. We therefore focus particular attention on solutions in which the core-valence Coulomb parameter is fixed at the same value of 7.9 eV for both compounds (Table III). For La_2CuO_4 we find that acceptable values for the satellite intensity and energy are best reproduced by a small positive Δ value of around 0.8 eV and a transfer integral T of 2.4 eV. These are in sensible agreement with values found elsewhere in the literature.[11,50,52] By contrast, for Nd_2CuO_4 two different sorts of solution are found. The first has a negative Δ value of -0.9 eV and a much reduced transfer integral $T = 1.2$ eV. The second solution, which we believe to be unphysical, has both T and Δ very much greater than for La_2CuO_4. The low satellite intensity and large value of W for Nd_2CuO_4 in relation to La_2CuO_4 is thus seen to be associated with a negative Δ value. This is not an artifact of constraining Q to be 7.9 eV: negative Δ values are obtained for all Q values in the range from 7.4 eV upward. In fact, solutions with a slightly reduced Q value for Nd_2CuO_4 are probably more physically realistic as they do not involve such a dramatic reduction in T (Table III). Following a discussion of the low value of the charge-transfer gap for Nd_2CuO_4 by Maekawa and co-workers,[37] the difference between La_2CuO_4 and Nd_2CuO_4 may be understood qualitatively as follows. The negative Madelung site potential at the Cu^{II} ion in a cuprate material destabilizes the Cu^{II} $3d$ levels relative to the O^{-II} $2p$ levels. This site potential is smaller for the four-coordinate Cu^{2+} environment in the T' structure of Nd_2CuO_4 than for the six-coordinate environment of the tetragonal T structure of La_2CuO_4. Thus the difference in Madelung energy between in-plane O^{2-} sites and Cu^{2+} sites is 46.37 eV for Nd_2CuO_4 and 49.22 eV for La_2CuO_4 (Ref. 38): a stabilization of the Cu $3d$ levels relative to the O $2p$ levels in Nd_2CuO_4 by 2.85 eV compared to the value in La_2CuO_4 is thus predicted by the ionic model. Given that $\Delta = 0.8$ eV for La_2CuO_4, a negative value of Δ for Nd_2CuO_4 is perfectly comprehensible. The stabilization of the $3d^{10}\underline{L}^1$ configuration relative to the $3d^9$ configuration is also important in raising the effective Cu^{II}/Cu^{I} redox potential within the T' structure and allowing for n-type doping by Ce^{IV}. Moreover, the in-plane Cu—O bond length is longer in Nd_2CuO_4 (1.98 Å) than in La_2CuO_4 (1.90 Å) and the transfer integral is expected to be somewhat smaller in the former compound. Maekawa has suggested that the transfer integral should scale as (1/bond length)^4 so that the reduction is not expected to be quite as dramatic as in Table III assuming $Q = 7.9$ eV for Nd_2CuO_4.

A negative Δ value has been inferred from the previous core-level study Nd_2CuO_4 by Ishii *et al.*, but was dismissed as physically unrealistic.[11] However, both Misokawa *et al.*[53] and Okada *et al.*[54] suggested a negative Δ value for the Cu^{III} compound $NaCuO_2$. There the ground state was dominantly $3d^9\underline{L}^1$ and the gap respon-

sible for the insulating nature of this compound was attributed to the p-p excitation

$$3d^9\underline{L}^1+3d^9\underline{L}^1\rightarrow 3d^9\underline{L}^2+3d^9 .$$

In the present context we are suggesting a dominant ground configuration $3d^{10}\underline{L}^1$ and a gap due to the excitation

$$3d^{10}\underline{L}^1+3d^{10}\underline{L}^1\rightarrow 3d^{10}\underline{L}^2+3d^{10} .$$

Moreover, electron doping is into states of dominant O $2p$ character so that the atomic nature of the n-type charge carriers in $Nd_{2-x}Ce_xCuO_4$ is proposed to be very similar to those of the p-type carriers in $La_{2-x}Sr_xCuO_4$. However, it should be emphasized that owing to the rather small absolute values of Δ and the strong ground-state mixing between the configurations, the conduction-band states retain very substantial Cu $3d$ character.

Turning next to the effects of doping, the striking feature of Fig. 14 is that the Cu $2p_{3/2}$ peak profile shows very little variation with Ce doping. This is emphasized in Fig. 15 which superimposes spectra for Nd_2CuO_4 and $Nd_{1.8}Ce_{0.2}CuO_4$. Remembering that we are dealing with reduced samples, the data agree in this respect with Ishii *et al.*[11] who studied vacuum-annealed samples in the composition range $0.10<x<0.20$. There is a clear discrepancy with the data of Klauda and co-workers.[14,15] The reasons for the experimental disagreement are unclear at present, although our surface preparation procedure is different from both of these other groups.

Assuming a Ce^{IV} valence, formal electron counting requires that, for a Ce doping level x, a fraction x of the Cu^{II} ions are converted to Cu^{I}. Although the extra electrons may be delocalized in the initial state for $x>0.10$, in the final state in XPS we envisage localization to give distinct final-state configurations associated with Cu^{I} ($3d^{10}$) and Cu^{II} ($3d^9$ and $3d^{10}\underline{L}^1$). The $3d^{10}$ and $3d^{10}\underline{L}^1$ configurations differ little in energy and therefore will both fall within the envelope of the main peak. We therefore expect a decrease in the intensity ratio I_s/I_m by a factor $1-x$, where x is the Ce doping level. The fact that this change is not observed is extremely puzzling. Okada, Seino, and Kotani[55] have considered the effects of doping electrons into essentially Cu $4s$-like states and have shown that this would lead to constant satellite intensity. However, this model is not consistent with the observed decrease in Cu $2p_{3/2}$ core-edge excitonic intensity in electron-energy-loss spectroscopy (EELS) observed on Th doping Nd_2CuO_4.[7] An alternative is that a fraction x of the Cu yields a $3d^{10}$ final state, but that for the remaining fraction $(1-x)$ of Cu ions the parameters T, Δ, and Q rescale in such a way that the intensity ratio between

$$I(3d^9)=(I_s)$$

and

$$[I(3d^{10})+I(3d^{10}\underline{L}^1)]=(I_m)$$

remains accidentally constant. For example, for $Nd_{1.8}Ce_{0.2}CuO_4$, this would imply that $I(3d^9)/I(3d^{10}\underline{L}^1)$ increases from the value of 0.26 for Nd_2CuO_4 itself to 0.33, the value of W remaining fixed. This is easily achieved with a small increase in Q and a decrease in Δ. Thus the data for $Nd_{1.8}Ce_{0.2}CuO_4$ can be fitted with $Q=8.0$ eV, $\Delta=-0.5$ eV, and $T=1.7$ eV. The actual values of these parameters are not in themselves important, but the general point that there is a strong dependence of satellite intensity and energy on the parameters of the Larsson-Sawatzky model means that it is dangerous to derive values of the $3d$ electron count from the core-level spectra without a critical consideration of the model involved.

Finally, we consider the effects of Sr substitution in La_2CuO_4. As shown in Fig. 16, Sr doping in this system leads to broadening on the high binding energy side of the main Cu $2p_{3/2}$ peak and a small shift to higher binding energy. There is, however, only a small change in the intensity ratio between the main peak and the satellite. The experimental picture here is in agreement with a number of previous papers including those of Nücker *et al.*[56] and Ishii *et al.*,[11] although these authors do not carry out the overlay of spectra necessary to highlight the main peak line broadening. However, our experimental data is very different from that of Rao and coworkers[57,58] who found a very pronounced decrease in satellite intensity with hole doping from the value $I_s/I_m=0.44$ for $x=0$ to $I_s/I_m=0.28$ for $x=0.15$. The reasons for the major experimental disagreements are unclear, although the Cu core-level spectra in the 1991 papers cannot be appraised either in relation to O $1s$ core-level data or valence-level spectra. We also have reservations about interpretation of data for the hole doped samples in terms of the Larsson-Sawatzky model with only two final-state configurations. As discussed in detail elsewhere,[53,59–61] the introduction of holes into a parent Cu^{II} compound allows the appearance of three new final-state valence shell configurations associated with the formal oxidation from Cu^{II} to Cu^{III}. These are $3d^8$, $3d^9\underline{L}^1$, and $3d^{10}\underline{L}^2$. The peaks associated with $3d^9\underline{L}^1$ and $3d^{10}\underline{L}^2$ overlap the high binding side of the $3d^9$ and $3d^{10}\underline{L}^1$ final-state configurations associated with Cu^{II}. The shift between the $d^{10}\underline{L}^1$ and $d^{10}\underline{L}^0$ configurations accounts for the broadening of the "main peak" of La_2CuO_4 on Sr doping. The intensity ratio I_s/I_m is now given by

$$I_s/I_m=[I(3d^9)+I(3d^9\underline{L}^1)]/[I(3d^{10}\underline{L}^1)+I(3d^{10}\underline{L}^2)] . \quad (8)$$

In the model Cu^{III} compound $NaCuO_2$, the configuration $3d^{10}\underline{L}^2$ dominates the spectra[53,54,62] and one cannot assume that, in general,

$$I(3d^9)/I(3d^{10}\underline{L}^1)=I(3d^9\underline{L}^1)/I(3d^{10}\underline{L}^2) . \quad (9)$$

Thus the two-configuration Larsson-Sawatzky model may be misleading when applied to hole doped cuprates.

IV. CONCLUDING REMARKS

The present study represents the first comprehensive study of valence and core levels in reduced $Nd_{2-x}Ce_xCuO_4$ by photoemission techniques on atomically clean surfaces. Electron doping leads to the appear-

ance of a measurable density of states at the Fermi energy in valence-region spectra, but, surprisingly, this is observed most clearly at the low-energy photon energy provided by Ne(I) radiation ($h\nu = 16.8$ eV). Ce core-level spectra indicate that across the complete composition range, Ce substitutes as Ce^{IV}. The low satellite intensity and large satellite to main peak separation in Cu $2p$ XPS are shown to be consistent with the Larsson-Sawatzky model, assuming a negative Δ value. This in turn implies that Nd_2CuO_4 should perhaps be regarded as a p-p insulator, rather than a charge-transfer insulator, although in view of the close energy matching between $3d^9$ and $3d^{10}\underline{L}^1$ ground-state configurations the importance of this distinction should not be overemphasized.

ACKNOWLEDGMENTS

We are grateful to P. A. Cox for a number of stimulating conversations and to O. Cohen and F. H. Potter for help with numerical aspects of the Larsson-Sawatzky model.

[1]Y. Tokura, H. Takagi, and S. Uchida, Nature **337**, 345 (1989).
[2]H. Takagi, S. Uchida, and Y. Tokura, Phys. Rev. Lett. **62**, 1197 (1989).
[3]M. E. Lopez-Morales, R. J. Savoy, and P. M. Grant, Solid State Commun. **71**, 1079 (1989).
[4]J. Zaanen, G. A. Sawatzky, and J. W. Allen, Phys. Rev. Lett. **55**, 418 (1985).
[5]*Standard Potentials in Aqueous Solution,* edited by A. J. Bard, R. Parsons, and J. Jordan (Marcel Dekker, New York, 1985).
[6]N. Nücker, P. Adelmann, M. Alexander, H. Romberg, S. Nakai, J. Fink, H. Rietschel, G. Roth, H. Schmidt, and H. Spille, Z. Phys. B **75**, 421 (1989).
[7]M. Alexander, H. Romberg, N. Nücker, P. Adelmann, J. Fink, J. T. Markert, M. B. Maple, S. Uchida, H. Takagi, Y. Tokura, A. C. W. P. James, and D. W. Murphy, Phys. Rev. B **43**, 333 (1991).
[8]J. Tranquada, S. Heald, A. R. Moodenbaugh, G. Liang, and M. Croft, Nature **337**, 720 (1989).
[9]E. E. Alp, S. M. Mini, M. Ramanathan, B. Dabrowski, D. R. Richards, and D. G. Hinks, Phys. Rev. B **40**, 2617 (1989).
[10]E. Lederman, L. Wu, M. L. denBoer, P. A. van Aken, W. F. Müller, and S. Horn, Phys. Rev. B **44**, 2320 (1991).
[11]H. Ishii, T. Koshizawa, H. Kataura, T. Hanyu, H. Takai, K. Mizoguchi, K. Kume, I. Shiozaki, and S. Yamaguchi, Jpn. J. Appl. Phys. **28**, L1952 (1989).
[12]T. Suzuki, M. Nagoshi, Y. Fukuda, K. Oh-ishi, Y. Syono, and M. Tachiki, Phys. Rev. B **42**, 4263 (1990).
[13]A. Fujimori, Y. Tokura, H. Eisaki, H. Takagi, S. Uchida, and E. Takayama-Muromachi, Phys. Rev. B **42**, 325 (1990).
[14]A. Grassmann, J. Ströbel, M. Klauda, J. Schlötterer, and G. Saemann-Ischenko, Europhys. Lett. **9**, 827 (1989).
[15]M. Klauda, J. P. Ströbel, J. Schlötterer, A. Grassmann, J. Markl, and G. Saemann-Ischenko, Physica C **173**, 109 (1991).
[16]G. Liang, J. Chen, M. Croft, K. V. Ramanujachary, M. Greenblatt, and M. Hedge, Phys. Rev. B **40**, 2646 (1989).
[17]S. Kohiki, J. Kawai, T. Kamada, S. Hayashi, H. Adachi, K. Setsune, and K. Wasa, Solid State Commun. **73**, 787 (1990).
[18]M. K. Rajumon, D. D. Sarma, R. Vijayaraghavan, and C. N. R. Rao, Solid State Commun. **70**, 875 (1989).
[19]J. W. Allen, C. G. Olson, M. B. Maple, J.-S. Kang, L. Z. Liu, J.-H. Park, R. O. Anderson, W. P. Ellis, J. T. Markert, Y. Dalichaouch, and R. Liu, Phys. Rev. Lett. **64**, 595 (1990).
[20]Y. Sakisaka, T. Maruyama, Y. Morikawa, H. Kato, K. Edamoto, M. Okusawa, Y. Aiura, H. Yanashima, T. Terashima, Y. Bando, K. Iijima, K. Yamamoto, and K. Hirata, Phys. Rev. B **42**, 4189 (1990).
[21]D. E. Fowler, C. R. Brundle, J. Lerczak, and F. Holtzberg, J. Electron Spectrosc. Relat. Phenom. **52**, 323 (1990).
[22]J. T. Markert and M. B. Maple (unpublished).
[23]R. G. Egdell, W. R. Flavell, and M. S. Golden, Supercond. Sci. Technol. **3**, 8 (1989).
[24]J. M. Tarascon, L. H. Greene, W. R. MacKinnon, G. W. Hall, and T. M. Geballe, Science **235**, 1373 (1987).
[25]A. J. Arko *et al.*, Phys. Rev. B **40**, 2268 (1989).
[26]T. Takahashi, F. Maeda, H. Katayama-Yoshida, Y. Okabe, T. Suzuki, A. Fujimori, S. Hosoya, S. Shamoto, and M. Sato, Phys. Rev. B **37**, 9788 (1988).
[27]Y. Hwu, M. Marsi, A. Terrasi, D. Rioux, Y. Chang, J. T. McKinley, M. Onellion, G. Margaritondo, M. Capozi, C. Quaresima, A. Campo, C. Ottaviani, P. Perfetti, N. G. Stoffel, and E. Wang, Phys. Rev. B **43**, 3678 (1991).
[28]B. Reihl, Y. Maeno, I. Mangelschots, K. O. Magnuson, and C. Rossel, Solid State Commun. **74**, 31 (1990).
[29]T. Arima, K. Kikuchi, M. Kasuya, S. Koshihara, Y. Tokura, T. Ido, and S. Uchida, Phys. Rev. B **44**, 917 (1991).
[30]J. J. Yeh and I. Lindau, At. Data and Nucl. Data Tables **32**, 1 (1985).
[31]M. P. Seah and W. A. Dench, Surf. Interface Anal. **1**, 2 (1979).
[32]R. G. Egdell and W. R. Flavell, Z. Phys. B **74**, 279 (1989).
[33]Z.-X. Shen, D. S. Dessau, B. O. Wells, C. G. Olson, D. B. Mitzi, L. Lombado, R. S. List, and A. J. Arko, Phys. Rev. B **44**, 12 098 (1991).
[34]R. G. Egdell, M. R. Harrison, M. D. Hill, L. Porte, and G. Wall, J. Phys. C **17**, 2889 (1984).
[35]H. Eisaki, S. Uchida, T. Misokawa, H. Namatame, A. Fujimori, J. van Elp, P. Kuiper, G. A. Sawatzky, S. Hosoya, and H. Katayama Uchida, Phys. Rev. B **45**, 12 513 (1992).
[36]F. C. Zhang and T. M. Rice, Phys. Rev. B **37**, 3759 (1989).
[37]S. Maekawa, Y. Ohta, and T. Tohyama, in *Physics of High-Temperature Superconductors,* edited by S. Maekawa and M. Sato (Springer-Verlag, Berlin, 1992), p. 29 and references therein.
[38]J. B. Torrance and R. M. Metzger, Phys. Rev. Lett. **63**, 1515 (1989).
[39]J. C. Fuggle, M. Campagna, Z. Zolnierek, R. Lässer, and A. Platau, Phys. Rev. Lett. **45**, 1597 (1980).
[40]A. F. Orchard and G. Thornton, J. Electron Spectrosc. Relat. Phenom. **13**, 27 (1978).
[41]P. Burroughs, A. Hamnett, A. F. Orchard, and G. Thornton, J. Chem. Soc., Dalton Trans. 1686 (1976).
[42]E. Wuilloud, B. Delley, W.-D. Schneider, and Y. Baer, Phys. Rev. Lett. **53**, 202 (1984).
[43]A. Kotani, T. Jo, and J. C. Parlebas, Adv. Phys. **37**, 37 (1988).
[44]T. Ikeda, K. Okada, H. Ogasawara, and A. Kotani, J. Phys. Soc. Jpn. **59**, 622 (1990).
[45]A. Fujimori, Phys. Rev. B **28**, 2281 (1983).
[46]A. Fujimori, Phys. Rev. B **28**, 4489 (1983).
[47]G. van der Laan, C. Westra, C. Haas, and G. Sawatzky, Phys.

Rev. B **23**, 4369 (1981).
[48]S. Larsonn, Chem. Phys. Lett. **32**, 401 (1975); **40**, 362 (1976).
[49]J. Ghijsen, L. H. Tjeng, J. van Elp, H. Eskes, J. Westerink, G. A. Sawatzky, and M. T. Czyzyk, Phys. Rev. B **38**, 11 322 (1988).
[50]A. Fujimori, E. Takayama-Muromachi, Y. Uchida, and B. Okai, Phys. Rev. B **35**, 8814 (1987).
[51]A. E. Bocquet, T. Mizokawa, T. Saitoh, H. Namatame, and A. Fujimori, Phys. Rev. B **46**, 3771 (1992).
[52]Z. Shen, J. W. Allen, J. J. Yeh, J. S. Kang, W. Ellis, W. Spicer, I. Lindau, M. B. Maple, Y. D. Dalichaouch, M. S. Torikachvili, J. Z. Sun, and T. H. Geballe, Phys. Rev. B **36**, 8414 (1987).
[53]T. Misokawa, H. Namatame, A. Fujimori, K. Akeyama, H. Kondoh, H. Kuroda, and N. Kosugi, Phys. Rev. Lett. **67**, 1638 (1991).
[54]K. Okada, A. Kotani, B. T. Thole, and G. A. Sawatzky, Solid State Commun. **77**, 835 (1991).
[55]K. Okada, Y. Seino, and A. Kotani, J. Phys. Soc. Jpn. **59**, 2639 (1990).
[56]N. Nücker, J. Fink, B. Renker, D. Ewert, C. Politis, P. J. W. Weijs, and J. Fuggle, Z. Phys. B **67**, 9 (1987).
[57]A. K. Santra, D. D. Sarma, and C. N. R. Rao, Phys. Rev. B **43**, 5612 (1991).
[58]C. N. R. Rao, Phil. Trans. Roy. Soc. London A **336**, 595 (1991).
[59]T. Gourieux, G. Krill, M. Maurer, M. F. Ravet, A. Menny, H. Tolentino, and A. Fontaine, Phys. Rev. B **37**, 7516 (1988).
[60]W. R. Flavell and R. G. Egdell, Phys. Rev. B **39**, 231 (1989).
[61]M. S. Golden, S. J. Golden, R. G. Egdell, and W. R. Flavell, J. Mater. Chem. **1**, 63 (1991).
[62]W. Herzog, M. Schwartz, H. Sixl, and R. Hoppe, Z. Phys. B **71**, 19 (1988).